Methods

Animals

Twelve ferrets (*Mustela putorius*) (four males and eight females) were used for this study. The animals' age ranged between 3 months and 2.3 years, and their weight was between 800 and 2060 g. Ten brains were processed for cyto- and myeloarchitectonic characteristics. MRI scans were taken *in vivo* for two animals, including the one whose brain was used for the brain atlas. This animal was a female 2 years and 3 months old, weighing 800 g. MRI scans of paraformaldehyde-fixed ferret heads and brains were recorded in two other 2-year-old female ferrets. Computer-aided X-ray tomography was performed on isolated skulls from two additional animals.

All experimental procedures were in accordance with the NIH Guide for the Care and Use of Laboratory Animals (2011) and the guidelines of the European Communities Council Directive (86/609/EEC) and were approved by the Animal Care Committee of Regierung Oberbayern, Bavaria, Germany (AZ 211-2531-29/93).

MR Imaging

For the *in vivo* MRI scans, the animals were anesthetized with an intraperitoneal injection of MMK (20 µg/kg medetomidine, 0.5 mg/kg midazolam, 10 mg/kg ketamine) and taped to a platform adapted for insertion into the MR scanner. MR *in vivo* scans were performed on an ACHIEVA 1.5T (Philips Medical Systems) at the Klinikum Rechts der Isar, Technical University of Munich, Munich, Germany, with the following parameters:

Software: Gyroscan PMS/DICOM 4.0 MR; Receiving coil: Micro-47; Slice thickness: 150 µm; MRI sequence: 3dTSE/t1 (TR: 300 ms; TE: 25 ms; FA: 90°); Acquisition matrix: 256 × 256 pixel^2.

Images were reconstructed using Gyroscan PMS/DICOM 4.0 MR (Philips Medical Systems) and exported in DICOM format. The open-source program AMIDE: A Medical Imaging Data Examiner (amide.exe 1.0.4, © Andreas Loening, http://amide.sourceforge.net) was used to align the atlas brain MR scan in stereotaxic coordinates, and to bring the skull CT in register to the atlas brain.

The MRI scan at high resolution was performed on the entire head of a perfusion-fixed animal (described below in "Histology") in a Bruker 9.4 T scanner (Bruker AVANCE, Billerica, MA, USA) at the Medical Department of the University of North Carolina at Chapel Hill (UNC), Chapel Hill, NC, USA. A volume coil of 35 mm diameter was used for excitation and signal reception. Images were recorded using the rapid acquisition with relaxation enhancement (RARE) sequence with the following parameters:

Repetition time (TR) = 200 ms; Echo time (TE) = 9.94 ms; RARE factor = 1; Number of averages = 16; Matrix size = 544 × 400 × 256; Field of view (FOV) = 80 × 80 µm^2; Slice thickness = 80 µm.

All MRI/CT images shown in the atlas were extracted and exported with AMIDE software.

CT Imaging

The isolated skulls were scanned with the CT functionality of a NanoSPECT/CT scanner (Mediso Ltd., Budapest, Hungary) at the Leibniz Institute for Neurobiology (LIN), Magdeburg (Germany). CT scans were made at 45 kVp, 1.77 µA, with 180 projections, 500 ms per projection, and 96 µm pixel size. Images were reconstructed and aligned with the open-source program AMIDE.

S. Radtke-Schuller, *Cyto- and Myeloarchitectural Brain Atlas of the Ferret (Mustela putorius) in MRI Aided Stereotaxic Coordinates*, https://doi.org/10.1007/978-3-319-76626-3_2

Histology

Brains for histological processing were fixed by intracardial perfusion. Animals were initially anesthetized with an intraperitoneal injection of MMK (20 µg/kg medetomidine, 0.5 mg/kg midazolam, 10 mg/kg ketamine) before being lethally anesthetized with an overdose of sodium pentobarbital. When a deep anesthetic state marked by a complete loss of the flexor reflex at all limbs was reached, animals were perfused transcardially. After the injection of 500 I.U. of heparin directly into the left ventricle, 250 mL of phosphate-buffered saline (0.1 M PBS, pH 7.4 with 0.1% heparin) was infused, followed by 750 mL of 4% PFA (in 0.1 M PBS, pH 7.4). The brains were postfixed in the skull in 4% paraformaldehyde (PFA) in 0.1 M PBS (pH 7.4) at 4 °C for at least 7 days before removal, to best preserve the brain shape.

For the high-quality *ex vivo* MR scans, the ferrets were perfused and postfixed as described above, with the addition of 5% Magnevist® (Bayer HealthCare Pharmaceuticals Inc, Wayne, NJ, USA) in the fixation solution.

The brains for histological processing were cryoprotected in 30% sucrose in PBS (0.1 M, pH 7.4) until they sank to the bottom of the jar in this solution. Subsequently they were embedded (see below), shock-frozen in crushed dry ice, and cut in a cryostat (LEICA CM 3050S) into four series of 50-µm-thick frontal sections. The sections were directly mounted on gelatin-coated slides and air-dried overnight. Alternating section series were stained on slide, either for cells (Nissl) or for myelin (Gallyas 1979).

Atlas Coordinate System

The coordinate system of the ferret brain atlas is based on the conventional definition of anatomical sectioning planes so that frontal sections are cut perpendicular to the anterior-posterior axis of the brainstem (Fig. 1c). In the ferret, the brainstem axis is parallel to the horizontal tangential plane passing through the most dorsal points of the forebrain in its anterior and posterior parts, and the most dorsal point of the cerebellum. This plane (Fig. 1a, c) is chosen as the origin for the dorsoventral dimension, with negative values in the ventral direction. The lateral dimension is zeroed to the midsagittal plane (Fig. 1b), with negative values towards the right side and positive values towards the left side. The anterior-to-posterior coordinates of the atlas are indicated relative to the occipital crest used as a skull landmark and are valid for the skull and brain (head) in standard atlas orientation.

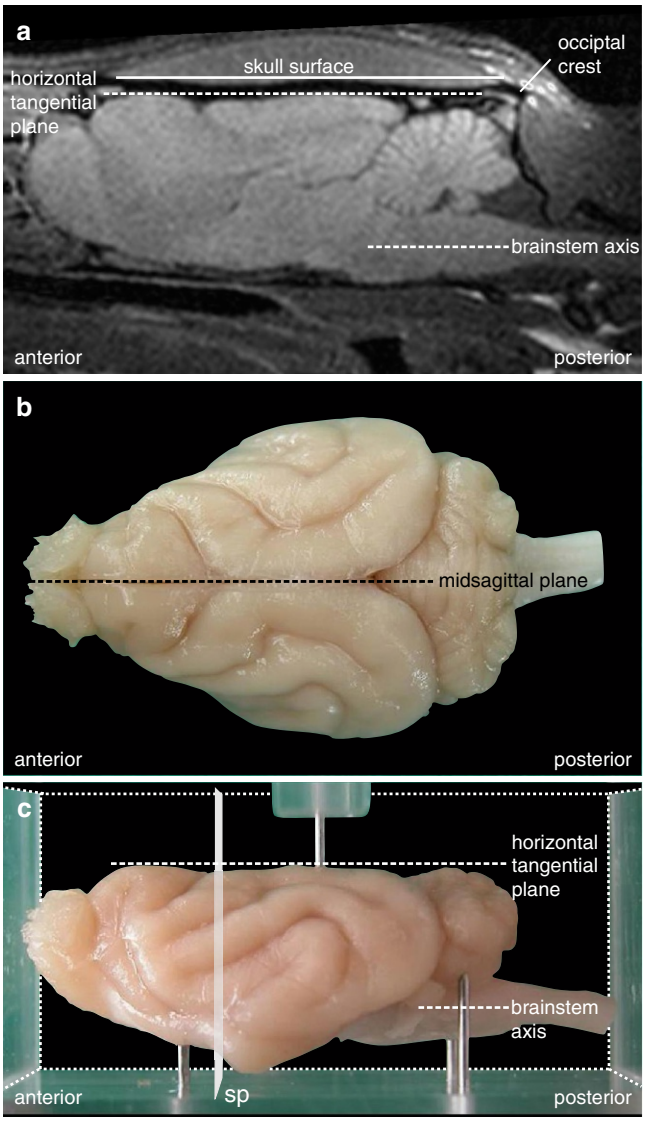

Fig. 1 Atlas coordinate system. (**a**) Parasagittal view of *in vivo* MR image of the atlas brain in standard orientation at 1000 µm off midline. The horizontal tangential plane (*stippled*) connecting the most dorsal points of the rostral and caudal cerebrum and the most dorsal elevation of the cerebellum at the midsagittal level (not seen) defines the horizontal dimensions of the atlas coordinate system. The horizontal tangential plane is parallel to the brainstem axis and the tangential plane connecting the most dorsal skull points overlying the forebrain (*solid line*). The occipital crest is a characteristic landmark of the skull and is used as the origin in the anterior-posterior direction. (**b**) The midsagittal line in a top view of the brain. (**c**) A fixed ferret brain positioned in the acrylic glass box for embedding (rectangular block volume indicated by *fine dotted lines*). The brain is positioned on three pins protruding from the base so that the horizontal tangential plane (as defined in the text) is aligned parallel to the base. A pin protruding from a bracket over the side walls of the box (only partly shown) holds the brain in place when the embedding medium is poured into the box. After embedding, the anterior and posterior surfaces of the block define the frontal sectioning plane (sp) perpendicular to both axes

Standardized Embedding

Ferret brains were sectioned in the standard frontal plane of the atlas following a standardized embedding protocol that has already proved useful for other small mammalian brains, including bats (Schuller et al. 1986) and gerbils (Radtke-Schuller et al. 2016). It uses a cuboid acrylic glass box adapted to the dimensions of the ferret brain (Fig. 1c). The fixed brain can easily be oriented on three adjustable supporting needles protruding from the bottom so that the horizontal tangential plane and the brainstem axis of the brain are parallel to the base of the box. The midsagittal plane is aligned with the long axis of the box. The brain is stabilized in this orientation by a needle sticking out from a bracket at the top of the box. The transparency of the box allows for photographic documentation of the embedding position before the embedding medium, a mixture of gelatin-albumin with freshly added glutaraldehyde, is poured into the space around the brain. After a hardening time of several minutes (minimum 3 min), the block can easily be taken out of the box after the needles have been retracted and the walls have been disassembled. The block is shock frozen in crushed dry ice and mounted with its surface facing the caudal end of the brain on the cutting platform of a cryostat (LEICA CM 3050S, Leica Biosystems, Wetzlar, Germany). Due to the prior alignment of the brain within the box, the resulting sectioning plane corresponds to the standard frontal plane.

Sectioning the brain in the standard atlas plane is also possible without an embedding chamber, if only part of the brain is to be sectioned. The brain portion of interest can be mounted directly on the cryostat holder and coated with a cryo-embedding medium. For this simplified procedure, the atlas frontal sectioning plane can be achieved by positioning the brain upside down on a flat surface so that the base makes up for the tangential plane of the atlas coordinate system. With a cut perpendicular to the base and the midsagittal plane of the brain, a surface for mounting the brain's portion of interest on the cryostat platform is created. Subsequent sectioning parallel to this cutting surface should result in sections corresponding to the frontal plane of the atlas.

Stereotaxic Reference System

Stereotaxic procedures rely on the use of external skull landmarks accessible during experiments and the availability of a brain atlas that links these external landmarks to the internal coordinate system of the brain. Skull landmarks that are traditionally used in rodents, such as the bregma and lambda, are either difficult to determine and interindividually variable in young ferrets or not detectable at all in adult ferrets, so the reliability of these landmarks is substantially reduced. Interaural coordinates are also difficult to determine in experimental animals because of the oblique orientation of the external meatuses (Fig. 2, bottom).

The occipital crest at a given lateral distance to the midline is the most distinctive and most easily accessible skull

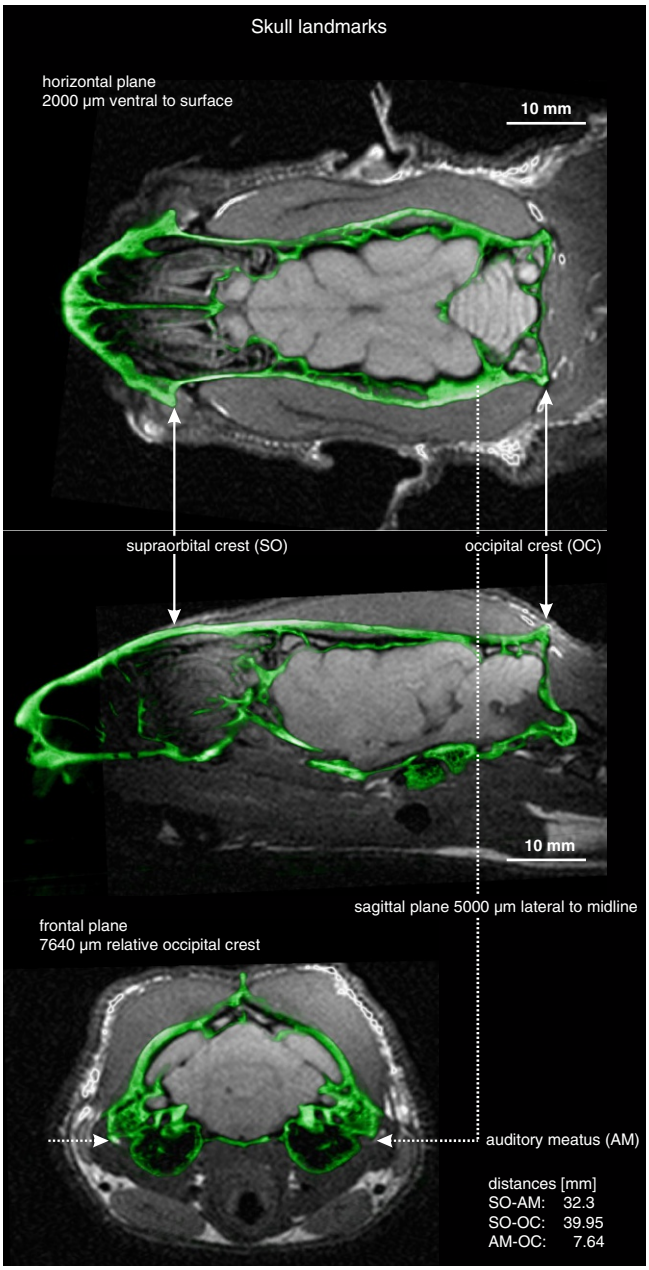

Fig. 2 Characteristic skull landmarks. Characteristic landmarks of the ferret's skull are depicted in an overlay of *in vivo* MRI (*gray*) and CT (*green*) images in different planes (top, horizontal; middle, parasagittal; bottom, frontal). The most distinct and most easily accessible landmark is the occipital crest, which is used as the anterior-posterior origin in the stereotaxic coordinate system. Scale applies to all images

landmark (Fig. 2, top and middle) and is therefore the landmark of choice for anterior-posterior reference. The left–right symmetry and the rostro-caudal tilt adjustment of the skull *in vivo* according to the atlas reference system are best achieved by the measurement of a mediolateral and parasagittal profile line of the skull, a profile-oriented stereotaxic procedure (Schuller et al. 1986).

The specific pattern of skull profiles also gives hints as to the overall length of the skull, which can be used for eventual recalibration of the rostro-caudal coordinates for different head and brain sizes. The skull and brain sizes differ considerably with weight and gender in individual adult ferrets (Lawes and Andrews, 1987), accounting for the inherent difficulty of this procedure. Such calibration could theoretically also use the rostro-caudal distance between the supraorbital processes (Fig. 2, top) and the occipital crest as proposed by Lawes and Andrews (1987), but practically the supraorbital process is inaccessible in experiments.

Selection of the Atlas Series

The specific atlas series was chosen for two reasons: (1) the good tissue preservation and staining quality of the entire series of sections alternately stained for cell bodies (Nissl) and myelin (Gallyas) and (2) the availability of an *in vivo* MR scan of the animal's brain. The *in vivo* MR images were used as templates that made it possible to correct the histology sections for unavoidable distortions due to prior processing.

To assess how representative the chosen atlas brain is within the available pool of the ferret brain series (N = 10), the rostro-caudal location of characteristic brain structures was evaluated and compared between series. Figure 3 illustrates the indicative structures used: the rostral beginning of the neocortex (1), the center of the midline crossing of the anterior commissure (2), the rostral appearance of the posterior commissure (3), the genu of the facial nerve (4), the

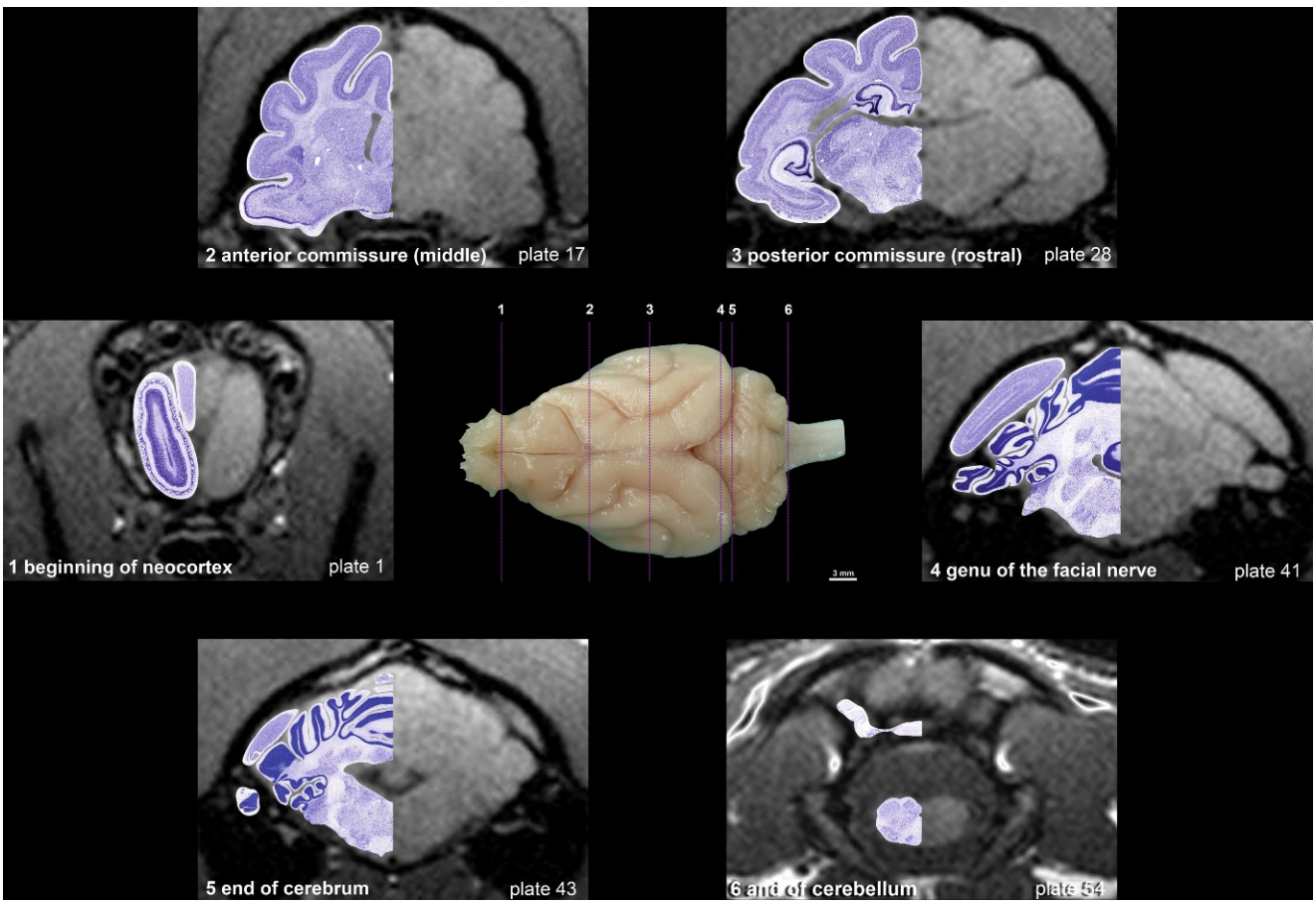

Fig. 3 Indicative structures in histological and MRI brain series. The following structures were used for interindividual comparison: beginning of neocortex (1), anterior commissure at midline crossing (2), rostral appearance of the posterior commissure (3), genu of the facial nerve (4), end of cerebral hemispheres (5), and end of the cerebellum (6). Montages combine *in vivo* MR images and half of the corresponding Nissl-stained section. The anterior-posterior locations of the corresponding atlas plates (plate number at bottom right corner) are indicated by dotted lines in the central brain image

caudal end of the cerebrum (5), and the caudal end of the cerebellum (6). Among these structures, the anterior and posterior commissure and the genu of the facial nerve could be determined with the highest accuracy (Fig. 4), so these represent the most reliable landmarks for interindividual comparison.

The coordinates of the anterior commissure were used as the common reference point for comparison and the coordinate values of the other structures were adjusted accordingly.

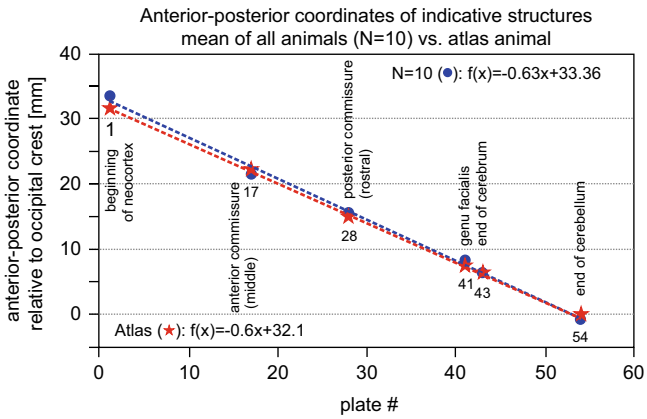

Fig. 4 Comparison of anterior-posterior location of indicative structures between atlas brain and group average. The anterior-posterior positions of the six indicative structures of Fig. 3, averaged over all investigated brains ($N = 10$) (*blue circles*) and the atlas brain (*red stars*). The *dashed lines* are the linear regression lines of these data (equations indicated below and above)

In Fig. 4, the rostro-caudal coordinates of the characteristic structures averaged over the ten animals (blue symbols and trend line) are represented in comparison with that of the atlas series (red symbols and trend line) as a function of the anterior-posterior coordinate (plate number). The slope and the constant term of the average trend line are slightly higher than in the atlas brain (slope, absolute value: 6.3 versus 6.0; constant term: 33.36 versus 32.1) and indicate that the atlas brain belongs to the overall shorter individuals in our sample.

When the animal's sex is taken into account, the overall length as measured from the first forebrain slice to the last cerebellum slice is about 110% larger for the four males (average 35.94 mm; standard deviation: 1.04) than for the six females (average 32.81 mm; standard deviation: 2.66) (Table 1). Within the group of six females, the overall length of the atlas brain (31.8 mm) is also smaller than the average (32.81 mm), being approximately 97% of average size. A comparison of the bicommissural space (the distance between the anterior commissure and the posterior commissure) in the different subgroups essentially shows the same pattern as for the overall distance (Table 1).

Our small sample size of ten brains is not sufficient to judge the significance of these values, but it does give an idea of how to position the atlas brain dimensions within the variation range of individual ferret brain sizes of our sample.

Table 1 Comparison of overall brain length and bicommissural space of females and males

	Atlas brain	All animals ($N = 10$)	Females ($n = 6$)	Males ($n = 4$)	Minimum	Maximum
Overall brain length (average), mm	31.8	34.06	32.81	35.94	30.39 (female)	37.6 (male)
Bicommissural space (ca−cp), mm	5.6	5.9	5.77	6.12	4.8 (female)	7.65 (male)

ca anterior commissure, *cp* posterior commissure

Preparation of Images and Plates

The *in vivo* MRI scan of the atlas brain was aligned according to the standard atlas coordinate system. The series consists of 150-µm-thick frontal slices extracted at 300 µm intervals. For each MRI slice, the matching Nissl-stained section of the histological atlas series was taken and grouped with the adjacent myelin-stained section. Every second triple of MRI, Nissl-stained, and myelin-stained sections was taken for the atlas and constitutes one of the 57 plates at 600 µm intervals (see Fig. 3 in chapter "Surface Views of the Ferret Brain"). The anterior-to-posterior coordinates of the plates are indicated relative to the occipital crest. Nissl and Gallyas sections were semiautomatically imaged at 10× magnification with a VS120 S1 virtual slide microscope at the Biology Department of the Ludwig-Maximilians-University (LMU) in Munich, Germany (VS120 S1: Olympus BX61VST, Olympus-Deutschland, Hamburg, Germany). Recording and file conversion were organized with dotSlide®, the proprietary software of the microscope (Olympus). The images were transformed from the virtual slide imaging format (.VSI) into a format (PDF) readable by Photoshop software (CS6, Adobe Systems, San Jose, CA, USA), which was used for image editing. Contrast and brightness were adjusted and the embedding background was manually removed from the images. To eliminate distortions of histological sections due to mounting and processing, sections were carefully adjusted to optimize the congruency of anatomical structures with the *in vivo* MRI. Slight differences between the adjusted histology sections and the corresponding MR images do remain and can be judged by the overlay of the structural delineations onto the *in vivo* MRIs, as represented on the abbreviation pages of the atlas.

The corrected histological sections in register with the MR images were compiled with the stereotaxic frame to form the atlas plates, using the CorelDRAW graphics suite (version X6 or X7, Corel Corporation, Ottawa, ON, Canada). Outlines of the brain and delineations of brain structures were drawn on the basis of the Nissl-stained sections on a superimposed layer. They match the structures seen in neighboring myelin-stained sections generally well, but not perfectly. This discrepancy is due to the slight shift in anterior-posterior location of the fiber-stained sections and the staining procedures, which altered the slices differently.

High-Quality MRI Series

A high-resolution MRI scan was aligned to the atlas coordinate system and resliced into frontal slices 150 µm thick. Four slices span the space between two consecutive atlas plates and are compiled on a separate MRI page for each plate. Contrast in the MR images was adjusted to optimize the salience of structural details for comparison with the histology sections. In the first of the four slices, the most clearly visible anatomical structures were labeled.

The correspondence of structures in MRI slices and histology sections is often evident. Nevertheless, the ability to identify in MR images the details recognized in the histology sections is limited, in spite of the advantages of the MR imaging method. Combining both methods maximizes the profit of each. Differences between the atlas brain images and the high-resolution MR images can be due to individual differences between the brains, to the fixation of the *ex vivo* versus the *in vivo* status, or a combination of both.

Anatomical Structures, Nomenclature, and Abbreviations

Anatomical structures were identified on the basis of cyto- and myeloarchitecture and their relative locations. Additional brain series stained for chemo- and immunoarchitecture (cytochrome oxidase, acetylcholine-esterase, NADPH-diaphorase, calcium-binding proteins (parvalbumin, calbindin, and calretinin), chondroitin sulfate proteoglycan (CSPG), neurofilament protein (SMI-32), and zinc stain (TIMM)) were consulted to support the structural identification. For this purpose, it proved especially useful to view anatomical structures in high-resolution MR images at various sectioning planes.

Although the number of explicit neuroanatomical publications on the ferret brain is limited, studies including neuroanatomical information implicitly were found more often and also used for delineations. Some names of brain structures were adopted from dog and cat studies. As no unified neuroanatomical nomenclature exists to date (Swanson 2015), the widely accepted Paxinos nomenclature and abbreviations for naming structures was used (as far as applicable) to ease comparison between species, including the rat (Paxinos and Watson 2013, Paxinos et al. 2009), mouse (Franklin and Paxinos 2012, Watson and Paxinos 2010), and monkey (Paxinos et al. 2008).

Functional denotations and already established ferret-specific terms were adopted accordingly and also mapped onto the atlas sections (names in italic characters) and onto the brain surface in Fig. 2 of chapter "Surface Views of the Ferret Brain" as far as their location could be deduced from ferret literature. Personal unpublished connectivity data were additionally considered.

Further References Taken into Account

Atlases of Carnivore Brains

Berman (1968) The brain stem of the cat: a cytoarchitectonic atlas with stereotaxic coordinates; **Berman and Jones** (1982) The thalamus and basal telencephalon of the cat: a

cytoarchitectonic atlas with stereotaxic coordinates; **Reinoso-Suárez** (1961) Topographischer Hirnatlas der Katze für experimental-physiologische Untersuchungen; **Snider and Niemer** (1964) A stereotaxic atlas of the cat brain; **Stolzberg *et al.*** (2017) Catlas: A magnetic resonance imaging-based three-dimensional cortical atlas and tissue probability maps for the domestic cat (*Felis catus*); **Adrianov and Mering** (1964) Atlas of the canine brain; **Montie *et al.*** (2009) Neuroanatomy and volumes of brain structures of a live California sea lion (*Zalophus californianus*) from magnetic resonance images.

Telencephalon

Cerebral Cortex

For the ferret-specific sulci and gyri (see Fig. 1 in chapter "Surface Views of the Ferret Brain"), we refer to the well-established names proposed by **Nigel *et al.*** (1998) with the exception of the frontal cortex, for which the nomenclature of the dog (**Kreiner** 1961) was adopted. Ferrets (*Mustelidae*) belong to the doglike carnivores of the two superfamilies of the order Carnivora, caniforms and feliforms (**Agnarsson *et al.*** 2010), and in some respects the ferret's neocortex, especially the frontal cortex, resembles that of the dog more than that of the cat.

Brodmann (1909) Vergleichende Lokalisationslehre der Großhirnrinde (includes *Cercoleptes);* **Danckers** (2003) Cytoarchitektonische Arealisierungen des Neocortex beim Mink (*Mustela vison*) und vergleichend-quantitative Untersuchungen zwischen der Wild- und Haustierform; **Kroenke *et al.*** (2014) Neuroanatomy of the ferret brain with focus on the cerebral cortex; **Zilles** (1985) The cortex of the rat.

Frontal Cortex

Craig *et al.* (1982) The thalamo-cortical projection of the nucleus submedius in the cat; **Duque and McCormick** (2010) Circuit-based localization of ferret prefrontal cortex; **Fritz *et al.*** (2010) Adaptive, behaviorally gated, persistent encoding of task-relevant auditory information in ferret frontal cortex; **Hassler and Muhs-Clement** (1964) Architektonischer Aufbau des sensomotorischen und parietalen Cortex der Katze; **Kreiner** (1961) The myeloarchitectonics of the frontal cortex of the dog; **Kreiner** (1964) Myeloarchitectonics of the perisylvian cortex in dog; **Kreiner** (1970) Homologies of the fissural patterns of the hemispheres of dog and cat; **Markowitsch *et al.*** (1978) The prefrontal cortex of the cat: anatomical subdivisions based on retrograde labelling of cells in the mediodorsal thalamic nucleus; **Musil and Olson** (1988a) Organization of cortical and subcortical projections to medial prefrontal cortex in the cat; **Öngür and Price** (2000) The organization of networks within the orbital and medial prefrontal cortex of rats, monkeys and humans; **Reep** (1984) Relationship between prefrontal and limbic cortex: A comparative anatomical review; **Stanton *et al.*** (1986) Thalamic afferents to cytoarchitectonic subdivisions of area 6 on the anterior sigmoid gyrus of the dog: A retrograde and anterograde tracing study; **Tanaka *et al.*** (1981) Corticostriate projections from the primary motor cortex in the dog; **Zhou *et al.*** (2016b) Dorsolateral frontal cortex of the ferret encodes perceptual difficulty during visual discrimination.

Parietal Cortex

Burton *et al.* (1982) Second somatic sensory area in the cerebral cortex of cats: somatotopic organization and cytoarchitecture; **Foxworthy *et al.*** (2013) Laminar and connectional organization of a multisensory cortex; **Foxworthy and Meredith** (2011) An examination of somatosensory area SIII in ferret cortex; **Kaas and Stepniewska** (2016) Evolution of posterior parietal cortex and parietal-frontal networks for specific actions in primates; **Keniston *et al.*** (2009) Somatosensory and multisensory properties of the medial bank of the ferret rostral suprasylvian sulcus; **Leclerc *et al.*** (1993) Electrophysiological examination of the representation of the face in the suprasylvian gyrus of the ferret: a correlative study with cytoarchitecture; **Manger *et al.*** (2002) Areal organization of the posterior parietal cortex of the ferret (*Mustela putorius*); **McLaughlin *et al.*** (1998) Organization of the forepaw representation in ferret somatosensory cortex; **Rice *et al.*** (1993) Cytoarchitecture of the ferret suprasylvian gyrus correlated with areas containing multiunit responses elicited by stimulation of the face; **Sawyer *et al.*** (2016) Somatosensory brainstem, thalamus, and cortex of the California sea lion (*Zalophus californianus*); **Sellers *et al.*** (2016) Oscillatory dynamics in the frontoparietal attention network during sustained attention in the ferret.

Temporal Cortex

Atiani *et al.* (2014) Emergent selectivity for task-relevant stimuli in higher-order auditory cortex; **Bajo *et al.*** (2007) The ferret auditory cortex: Descending projections to the inferior colliculus; **Bizley *et al.*** (2005) Functional organization of ferret auditory cortex; **Bizley *et al.*** (2015) Cortico-cortical connectivity within ferret auditory cortex; **Hackett *et al.*** (2001) Architectonic identification of the core region in auditory cortex of macaques, chimpanzees, and humans; **Kosmal *et al.*** (2004) Cytoarchitecture and thalamic afferents of the sylvian and composite posterior gyri of the canine temporal cortex; **Manger *et al.*** (2004) Visual areas in the lateral temporal cortex of the ferret (*Mustela putorius*).

Occipital Cortex

Cantone *et al.* (2005) Feedback connections to ferret striate cortex: Direct evidence for visuotopic convergence of feedback inputs; **Henderson** (1987a) Cholinergic innervation of

ferret visual system; **Homman-Ludiye *et al.*** (2010) Immunohistochemical parcellation of the ferret (*Mustela putorius*) visual cortex reveals substantial homology with the cat (*Felis catus*); **Hupfeld *et al.*** (2007) Deficits of visual motion perception and optokinetic nystagmus after posterior suprasylvian lesions in the ferret (*Mustela putorius furo*); **Innocenti *et al.*** (2002) Architecture and callosal connections of visual areas 17, 18, 19 and 21 in the ferret (*Mustela putorius*); **Jarosiewicz *et al.*** (2012) Functional biases in visual cortex neurons with identified projections to higher cortical targets; **Kalia and Whitteridge** (1973): The visual areas in the splenial sulcus of the cat; **Law *et al.*** (1988) Organization of primary visual cortex (area 17) in the ferret; **Philipp *et al.*** (2006) A motion-sensitive area in ferret extrastriate visual cortex: An analysis in pigmented and albino animals; **Rockland** (1985) Anatomical organization of primary visual cortex (area 17) in the ferret; **Symonds and Rosenquist** (1984) Corticocortical connections among visual areas in the cat.

Other

Bajo *et al.* (2014) The cholinergic basal forebrain in the ferret and its inputs to the auditory cortex; **Burwell** (2001) Borders and cytoarchitecture of the perirhinal and postrhinal cortices in the rat; **Clascá *et al.*** (1997) Insular cortex and neighboring fields in the cat: A redefinition based on cortical microarchitecture and connections with the thalamus; **Clascá *et al.*** (2000) Cortical connections of the insular and adjacent parietotemporal fields in the cat; **Dennis and Kerr** (1975) Olfactory bulb connections with basal rhinencephalon in the ferret: An evoked potential and neuroanatomical study ferret; **Groenewegen *et al.*** (1982) Cortical afferents of the nucleus accumbens in the cat, studied with anterograde and retrograde transport techniques; **Henderson** (1987b) Source of cholinergic input to ferret visual cortex; **Ino *et al.*** (2001) Projections from the hippocampal and parahippocampal regions to the entorhinal cortex. An anterograde and retrograde tract-tracing study in the cat; **Kelliher *et al.*** (2001) The ferret's vomeronasal organ and accessory olfactory bulb: Effect of hormone manipulation in adult males and females; **Kosmal *et al.*** (1997) Diversity of connections of the temporal neocortex with amygdaloid nuclei in the dog (*Canis familiaris*); **Krettek and Price** (1977) Projections from the amygdaloid complex to the cerebral cortex and thalamus in the rat and cat; **Manger *et al.*** (2005) The anterior ectosylvian visual area of the ferret: a homologue for an enigmatic visual cortical area of the cat?; **Musil and Olson** (1988b) Organization of cortical and subcortical projections to anterior cingulate cortex in the cat; **Olson and Musil** (1992) Topographic organization of cortical and subcortical projections to posterior cingulate cortex in the cat: Evidence for somatic, ocular, and complex subregions; **Patzke *et al.*** (2014) The claustrum of the ferret: afferent and efferent connections to lower and higher order visual cortical areas; **Ramsay and Meredith** (2004) Multiple sensory afferents to ferret pseudosylvian sulcal cortex; **Room and Groenewegen** (1986a) Connections of the parahippocampal cortex. I. Cortical afferents; **Room and Groenewegen** (1986b) Connections of the parahippocampal cortex in the cat. II. Subcortical afferents; **Woźnicka and Kosmal** (2003) Cytoarchitecture of the canine perirhinal and postrhinal cortex; **Woźnicka *et al.*** (2006) Cytoarchitectonic organization of the entorhinal cortex of the canine brain; **Witter *et al.*** (2000) Anatomical organization of the parahippocampal-hippocampal network.

Diencephalon

Thalamus

Angelucci *et al.* (1998) Brainstem inputs to the ferret medial geniculate nucleus and the effect of early deafferentation on novel retinal projections to the auditory thalamus; **Baldauf *et al.*** (2005) Ultrastructural analysis of projections to the pulvinar nucleus of the cat. I: Middle suprasylvian gyrus (areas 5 and 7); **Berson and Graybiel** (1978) Parallel thalamic zones in the LP-pulvinar complex of the cat identified by their afferent and efferent connections; **Graybiel and Berson** (1980) Histochemical identification and afferent connections of subdivisions in the lateralis posterior-pulvinar complex and related thalamic nuclei in the cat; **Herbert** (1963) Nuclear structure of the thalamus of the ferret; **Jimenez-Castellanos** (1949) Thalamus of the cat in Horsley-Clarke coordinates; **Jones** (1985) The thalamus; **Kaas and Lyon** (2007) Pulvinar contributions to the dorsal and ventral streams of visual processing in primates; **Kageyama and Wong-Riley** (1984) The histochemical localization of cytochrome oxidase in the retina and lateral geniculate nucleus of the ferret, cat, and monkey, with particular reference to retinal mosaics and ON/OFF-center visual channels; **Kosmal *et al.*** (2004) Cytoarchitecture and thalamic afferents of the sylvian and composite posterior gyri of the canine temporal cortex; **Lanciego and Vásquez** (2012) The basal ganglia and thalamus of the long-tailed macaque in stereotaxic coordinates. A template atlas based on coronal, sagittal and horizontal brain sections; **Pallas *et al.*** (1990) Visual projections induced into the auditory pathway of ferrets. I. Novel inputs to primary auditory cortex (AI) from the LP/pulvinar complex and the topography of the MGN-AI projection; **Ray and Price** (1993) The organization of projections from the mediodorsal nucleus of the thalamus to orbital and medial prefrontal cortex in macaque monkeys; **Restrepo *et al.*** (2002) Retinofugal projections following early lesions of the visual cortex in the ferret; **Stryker and Zahs** (1983) On and off sublaminae in the lateral geniculate nucleus of the ferret; **Sychowa** (1962) Medial geniculate body of the dog; **Winer**

et al. (2001) Projections of auditory cortex to the medial geniculate body of the cat; **Yu *et al.*** (2016) Structural and functional connectivity between the lateral posterior-pulvinar complex and primary visual cortex in the ferret.

Hypothalamus

Robarts and Baum (2007) Ventromedial hypothalamic nucleus lesions disrupt olfactory mate recognition and receptivity in female ferrets; **Wersinger and Baum** (1996) The temporal pattern of mating-induced immediate-early gene product immunoreactivity in LHRH and non-LHRH neurons of the estrous ferret forebrain; **Westwood** (1962) Anatomy of the hypothalamus of the ferret.

Brainstem

Bajo *et al.* (2007) The ferret auditory cortex: Descending projections to the inferior colliculus; **Bajo *et al.*** (2010) The non-lemniscal auditory cortex in ferrets: convergence of corticotectal inputs in the superior colliculus; **Billig *et al.*** (1999) Transneuronal tracing of neural pathways controlling an abdominal muscle, rectus abdominis, in the ferret; **Billig *et al.*** (2000) Definition of neuronal circuitry controlling the activity of phrenic and abdominal motoneurons in the ferret using recombinant strains of pseudorabies virus; **Boissonade *et al.*** (1993) Trigeminal nuclear complex of the ferret: Anatomical and immunohistochemical studies; **Carrive and Paxinos** (1994) The supraoculomotor cap: a region revealed by NADPH diaphorase histochemistry; **Hawthorn** (1985) A guide to the ferret brainstem; **Distler *et al.*** (2009) Retinal projections to the accessory optic system in pigmented and albino ferrets (*Mustela putorius furo*); **Doubell *et al.*** (2000) Topographical projection from the superior colliculus to the nucleus of the brachium of the inferior colliculus in the ferret: Convergence of visual and auditory information; **Henderson** (1987c) Overlap in the distribution of cholinergic and catecholaminergic neurons in the upper brainstem of the ferret; **Henderson and Sherriff** (1991) Distribution of choline acetyltransferase immunoreactive axons and terminals in the rat and ferret brainstem; **Henkel and Brunso-Bechtold** (1998) Calcium-binding proteins and GABA reveal spatial segregation of cell types within the developing lateral superior olivary nucleus of the ferret; **Henkel *et al.*** (2003) Quantitative measurement of afferent layers in the ferret inferior colliculus: DNLL projections to sublayers; **Horn *et al.*** (2009) The Edinger-Westphal nucleus represents different functional cell groups in different species; **Jian *et al.*** (2005) Afferent pathways to the region of the vestibular nuclei that participates in cardiovascular and respiratory control; **Meredith *et al.*** (2001) Organization of the neurons of origin of the descending pathways from the ferret superior colliculus; **Morest and Oliver** (1984) The neuronal architecture of the inferior colliculus in the cat: defining the functional anatomy of the auditory midbrain; **Nodal *et al.*** (2005) Development of the projection from the nucleus of the brachium of the inferior colliculus to the superior colliculus in the ferret; **Shintani *et al.*** (2003) Locations of neurons with respiratory-related activity in the ferret brainstem; **Thorpe and Herbert** (1976) The accessory optic system of the ferret; **Zhang *et al.*** (2002) Organization of the ferret lateral cervical nucleus and cervicothalamic tract; **Zhang and Hoffmann** (1993) Retinal projections to the pretectum, accessory optic system and superior colliculus in pigmented and albino ferrets.

Cerebellum

Glickstein *et al.* (2011) Functional localization in the cerebellum; **Jacqmot *et al.*** (2017) Comparison of several white matter tracts in feline and canine brain by using magnetic resonance diffusion tensor imaging; **Walberg *et al.*** (1979) The olivocerebellar projections to the flocculus and paraflocculus in the cat, compared to those in the rabbit; **Larsell** (1953) The cerebellum of the cat and the monkey; **Nigel *et al.*** (1998) Neuroanatomy of the ferret brain; **Provini *et al.*** (1998) Somatotopic nucleocortical projections to the multiple somatosensory cerebellar maps.